Coupling between mesosphere and ionosphere over Beijing through semidiurnal tides during the 2009 sudden stratospheric warming

Jiangang Xiong,[1,2] Weixing Wan,[1,2] Feng Ding,[1,2] Libo Liu,[1,2] Baiqi Ning,[1,2] and Xiaojuan Niu[3]

Received 5 January 2013; revised 5 April 2013; accepted 12 April 2013; published 15 May 2013.

[1] Sudden stratospheric warming (SSW) in the winter of 2008/2009 is the strongest recorded SSW event. The enhancement in semidiurnal variation of ionospheric TEC (total electron content) with phase shift forward is shown during 22 to 27 January 2009, based on the TEC observations in Beijing (40.30°N, 116.19°E geographic, 39.73°N dip latitude). We focus on finding the reason for the TEC variation. Winds observed by an all-sky meteor radar in the same observatory are used to study mesospheric variation. The semidiurnal solar tide in the mesosphere starts to increase before the SSW and maintains oscillation with period 16–20 days during the SSW. The semidiurnal lunar tides in TEC and wind start to increase on 17 and 15 January, respectively. Although the semidiurnal lunar tide in TEC over Beijing almost dies out on 1 February, that over equatorial ionospheric anomaly crest does not vanish until 15 February when lunar tide in wind tends to be very weak. The maximum of lunar tide in wind appears on 2 February at 96 km with amplitudes of 15 m/s and 21 m/s for zonal and meridional winds. The phase comparison shows that lunar tides in TEC and zonal wind reach their maxima at almost the same time, which is 2–4 h lag behind the meridional wind. The coupling between the mesosphere and ionosphere contributes to the semidiurnal variation of TEC through both solar and semidiurnal lunar tides. The enhancement in semidiurnal lunar tide is responsible for the TEC peak shift forward during the SSW.

Citation: Xiong, J., W. Wan, F. Ding, L. Liu, B. Ning, and X. Niu (2013), Coupling between mesosphere and ionosphere over Beijing through semidiurnal tides during the 2009 sudden stratospheric warming, *J. Geophys. Res. Space Physics*, *118*, 2511–2521, doi:10.1002/jgra.50280.

1. Introduction

[2] Sudden stratosphere warming (SSW) is a transient large-scale dynamical phenomenon lasting several days or weeks. It occurs in and strongly affects the entire winter stratosphere, causing significant variations in the mesosphere and thermosphere. SSW is induced by the interaction of planetary waves with the mean flow in the upper stratosphere [*Matsuno*, 1971]. The amplification of the quasi-stationary wave produces strong westward forcing in the winter stratosphere at high latitude which causes the reversal of the stratospheric jet and formation of a critical layer for the upward propagation quasi-stationary planetary waves. That could then induce a downward circulation in the stratosphere and an upward circulation in the mesosphere [*Liu and Roble*, 2002]. The downward circulation in the stratosphere causes adiabatic heating, and upward circulation in the mesopause causes adiabatic cooling around polar region at high latitude, i.e., the vertical circulations make the stratosphere warmer and the mesopause cooler at high latitude. The circulation may affect the low-latitude atmosphere [*Sathishkumar et al*., 2009]. Some results show that the circulation moving downward could cause heating of mesosphere at low latitude, but the mesopause cooling was also observed at the tropic region [*Shepherd et al*., 2007]. Observations also show that the stratosphere mesosphere system is dominated by some planetary waves such as 16 days and 22 days before and after onset of SSW [*Pancheva et al*., 2008]. The connection between the tropics and the pole during the SSW events is present through the quasi-16 day wave and the critical layer which progress towards the Pole [*Vineeth et al*., 2010].

[3] Many observations have shown that the ionosphere can have dramatic changes during and after a SSW event, such as ion temperature variation [*Goncharenko and Zhang*, 2008], total electron content (TEC) and electron density

[1]Key Laboratory of Ionospheric Environment, Institute of Geology and Geophysics, Chinese Academy of Sciences, Beijing, China.
[2]Beijing National Observatory of Space Environment, Institute of Geology and Geophysics, Chinese Academy of Sciences, Beijing, China.
[3]School of Physics & Information Engineering, Jianghan University, Wuhan, China.

Corresponding author: J. Xiong, Institute of Geology and Geophysics, Chinese Academy of Sciences, No. 19, Beitucheng Western Road, Chaoyang District, 100029, Beijing, China. (xjg@mail.iggcas.ac.cn)

2169-9380/13/10.1002/jgra.50280

profile variation [*Chau et al*., 2010; *Lin et al*., 2012; *Liu et al*., 2011], radio wave absorption [*Lasvtovilcvka and de la Morena*, 1987], semidiurnal variation of vertical drift [*Anderson and Araujo-Pradere*, 2010; *Chau et al*., 2009], reversal of the equatorial electrojet (EEJ) in the afternoon [*Sridharan et al*., 2009], etc. The model simulation shows the large zonal gradients of horizontal winds, and the zonal gradient of electric conductivities can produce large convergence or divergence of Hall and Pedersen currents, which in turn produces a polarization electric field and produces large ionospheric variability [*Liu et al*., 2010].

[4] In the second half of January 2009, a prominent SSW occurred, with temperature increasing more than 60 K in a few days at 10 hPa [*Manney et al*., 2009]. This SSW event is characterized by the extraordinary predominance of wave 2 in the stratosphere, and the remarkable development of the upper troposphere ridge over Alaska plays important roles in the SSW [*Harada et al*., 2010]. At Tromsø (69.6°N, 19.2°E) in Norway, temperature at 90 km shows a strong cooling of more than 50 K from 16 January [*Kurihara et al*., 2010]. At low latitude, lidar observations of temperature at Gadanki (13.5°N, 79.2°E) in India show an enhancement in the nightly mean temperature by 10–15 K at 70–80 km [*Sridharan et al*., 2010]. In the midlatitude, the simultaneous wind and temperature observations document the direct impact of the major SSW on the dynamic and thermal circulation of the mesopause region [*Yuan et al*., 2012]. Global OH and O_2 brightness in the mesosphere shows large variation [*Gao et al*., 2011]. Because the solar and geomagnetic activity is low during 2009 SSW, it is good for the study of ionospheric effects driven by processes from lower atmosphere. At Arecibo (18.34°N, 66.75°W) in Puerto Rico, the largest TEC perturbations occur during the daytime right after the SSW peak temperatures, and they last several days to weeks [*Chau et al*., 2010]. According to the TEC observation and vertical ion drift observation by Jicamarca radar, a semidiurnal change in the vertical ion drift produces the semidiurnal variation of TEC at low latitude with large amplitude during daytime, increasing in the morning and decreasing in the afternoon [*Goncharenko et al*., 2010a; *Goncharenko et al*., 2010b]. But there are opposite observations which show that TEC at high latitude increases in either the morning or afternoon sector [*Yue et al*., 2010].

[5] The most predominant features in the ionosphere during SSW is the enhanced semidiurnal variations, i.e., the increasing of upward vertical plasma drift in the morning and decreasing of upward vertical plasma drift even to downward in the afternoon, especially in the equatorial and low-latitude ionosphere [*Chau et al*., 2011]. Those changes are believed to be driven by wind changes in the ionospheric *E* region through *E* region dynamo. Although the reason of changes in the *E* region winds are not well known, model simulation by *Liu et al*. [2010] demonstrated that the enhanced quasi-planetary waves can produce changes in the semidiurnal solar tides in the stratosphere and mesosphere, which can lead to similar perturbations in the ionosphere. The absorption of ultraviolet radiation by ozone in the stratosphere is the most important tidal generation sources. The ozone density variation induced by the temperature changes during SSW and by the forcing circulation from planetary waves [*Goncharenko et al*., 2012] can also change the tidal winds in the stratosphere and, in turn, in the mesosphere. The semidiurnal perturbation in many ionospheric parameters such as TEC, vertical plasma drift, and EEJ possesses a phase shift to late local time [*Chau et al*., 2010; *Liu et al*., 2011]. Those phase variations in the ionosphere during SSW, which is connected to the moon phase, may be resulted from enhancement of semidiurnal lunar wave [*Fejer et al*., 2010]. The relation between the large lunar tide in the EEJ and the SSW may be suggested based on the observation of geomagnetic field of many years [*Stening*, 2011]. *Stening et al*. [1997] demonstrated that semidiurnal lunar tide in the middle and lower thermosphere (MLT) increased significantly during SSWs. The semidiurnal lunar tide in the Brazilian sector in the MLT region is observed to enhance during 2006 SSW [*Paulino et al*., 2012]. Recently, based on the mesospheric winds and EEJ observation at Tirunelveli (8.7°N, 77.8°E), *Sathishkumar and Sridharan* [2013] demonstrated that the large semidiurnal tide during 2009 SSW is mostly solar driven and only partly lunar driven in the low latitude. *Forbes and Zhang* [2012] demonstrated that the enhanced semidiurnal lunar tides in the mesosphere during 2009 SSW resulted from the resonance between lunar tides and a normal mode named Pekeris peak ,which shifted its peak to the lunar tidal period with strongly changed neutral winds during the SSW. The model simulation shows that the average semidiurnal lunar tide in the mesosphere increased with the largest enhancements about 60–70% at midlatitudes to high latitudes, which is greater than the enhancements in the migrating semidiurnal tide [*Pedatella et al*., 2012]. But model studies from the whole atmosphere model suggested that large changes in the migrating terdiurnal tide are responsible for the ionospheric perturbations, including amplitude variation and forward phase shift [*Fang et al*., 2012; *Fuller-Rowell et al*., 2010; *Fuller-Rowell et al*., 2011]. A combination study using model and satellite observation on the response of migrating tides to the SSW shows that the global electron density variation is related to an amplified semidiurnal migrating tide (SW2) in the lower thermosphere which results from changing background and redistribution ozone [*Jin et al*., 2012]. More comparisons between neutral winds and ionosphere variation are needed to distinguish the sources of ionospheric perturbations.

[6] Most of the above works based on the ground-based observations are on the response of mesosphere and ionosphere to the SSW in low or high latitudes. SABER/TIMED global observations and classical tidal theory all show that semidiurnal tide in MLT is stronger at midlatitudes than at low latitude [*Forbes and Zhang*, 2012; *Pedatella et al*., 2012]. It is important to compare semidiurnal variation in mesosphere and ionosphere during SSWs. In this study, we report response of mesosphere and ionosphere over Beijing (40.30°N, 116.19°E geographic, 39.73°N dip latitude) to the SSW in the winter 2008/2009. The tidal variation of winds in the mesosphere and TEC in the ionosphere and their possible relations will be discussed. We focus on explanation of enhancement in semidiurnal variation with maximum shift forward in TEC perturbation.

2. Data

[7] The wind data by an all-sky meteor radar is used to study the mesospheric wind and tide over Beijing. The radar

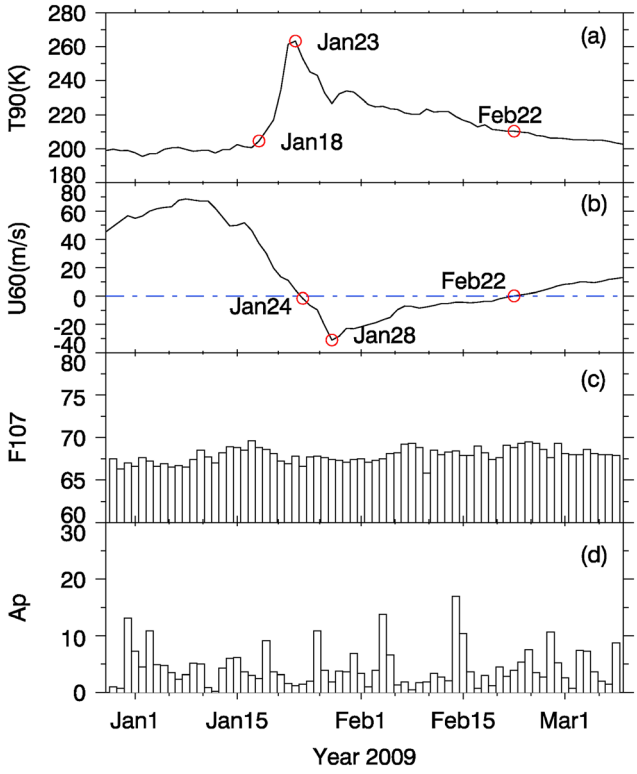

Figure 1. (a) Temperature at North Pole at 10 hPa (T90). (b) Zonal mean zonal wind at 60°N at 10 hPa. (c) Solar activity index F107. (d) Geomagnetic index Ap. The temperature starts to increase and reaches maximum at 18 and 23 January, respectively. Zonal mean zonal wind reverses from eastward to westward, reaches minimum, and recovers to eastward at 24 January, 28 January, and 22 February. Those dates are indicated by red circles.

operates at 38.5 MHz with a peak power of 7.5 kW. The radar is one of the four meteor radars along 120°E chain [*Yu et al*., 2012], but the other three radars were not working during the 2009 SSW. The radial wind velocity of meteor echo is estimated using correlation analysis. By assuming that the wind at a specified height and time window is uniform, the zonal wind (u) and meridional wind (v) can be determined by a least-squares fitting method [*Xiong et al*., 2004].

[8] The critical frequency (f_oF_2) and peak height (h_mF_2) of ionospheric *F* layer are measured by a CADI (Canadian Advanced Digital Ionosonde) located in Beijing. The TEC measured by a GPS receiver in Beijing is used to show ionospheric variation. The detail method to calculate vertical TEC from slant TEC and to calibrate the TEC can be found in *Ding et al*. [2012]. We also use GPS TEC from International GNSS (Global Navigation Satellite System) Service (IGS) global ionosphere maps to study the variation of TEC along the 120°E longitude during the 2009 SSW. The IGS-TEC data have a temporal resolution of 2 h and a spatial resolution of 2.5° in latitude and 5° in longitude.

[9] The zonal mean NCEP (National Center for Environmental Prediction) temperature and winds at 10 hPa is used to examine the features of the temperature and wind in the winter 2008/2009. The mesospheric temperature is from a Microwave Limb Sounder (MLS) of Earth Observing System (EOS) on board AURA, which was launched in 2004. The MLS on the AURA satellite scans the atmospheric limb continuously to measure temperature at tangent heights from the surface to 92 km [*Waters et al*., 2006]. AURA satellite is a polar orbit satellite; all profiles are obtained at two local times (~2.3 LT and ~13.3 LT). The zonal mean MLS/AURA temperatures at 40.30°N at 0.0215 hPa (~88 km) are used to show mesospheric temperature variation over Beijing.

3. Results

[10] Figure 1 displays the temperature and zonal mean zonal wind at 10 hPa from NCEP during the first 2 months of 2009. The solar activity index F107 and geomagnetic index Ap are shown in the last two panels of Figure 1. Polar stratosphere temperature starts to increase and reaches maximum at 18 and 23 January, respectively. Zonal mean zonal wind reverses from eastward to westward, reaches minimum, and recovers to eastward at 24 January, 28 January, and 22 February, respectively. The solar and geomagnetic activities are relatively quiet in January 2009 but with occasional minor disturbances in February.

3.1. Mesospheric Wind and Ionospheric Parameter Observations

[11] Mean zonal wind from 80 to 100 km in the mesosphere is shown in the upper panel of Figure 2. The critical frequency f_oF_2 and height h_mF_2 in the afternoon averaged from 12 to 16 local times, and zonal mean temperature at about 88 km observed by AURA at 2.3 LT are also shown in Figure 2. The zonal mean temperature at 70°N decreases from 15 January which is about 3 days before temperature increasing time at 10 hPa. It decreases 29 K from 209 K to 180 K during 15 January and 23 January. The temperature at 70°N recovers to 209 K at about 30 January. Although the temperature at 40.30°N decays slowly from about 10 January, the prominent drop of temperature starts from 22 January. It decreases about 10 K from 193 K to 183 K during 22 January to 26 January before it recovers to 193 K at about 29 January. The temperature decay from local observation may be larger than the decay of zonal mean temperature during SSW because of longitudinal variation by traveling planetary wave [*Hoffmann et al*., 2007]. For example, temperature at 90 km at Tromsø (69.6°N, 19.2°E) drops more than 50 K, and temperature at 90 km at Fort Collins (41°N, 105°W) drops 9 K in 1 day during 2009 SSW [*Kurihara et al*., 2010; *Yuan et al*., 2012]. The mean zonal wind decreases after 10 January. From 21 January, zonal wind reverses to easterly starting at 100 km then downward to 80 km. The downward propagation is at a rate of 4 km per day, which is slower than the rate at high latitude [*Kurihara et al*., 2010]. That means the impact of SSW on mesosphere over Beijing at midlatitude is smaller than on that over Tromsø at high latitude mesosphere. The zonal westward wind in the whole observation range persisted only for 5 days, much shorter than in stratosphere at 10 hPa as shown in Figure 1b. But the zonal wind reversal and recovery time in the mesosphere is earlier than that in stratosphere at high latitude.

[12] The ionosphere also shows large variation before and after the peak of the SSW when the solar and geomagnetic activities are low. In the afternoon, f_oF_2 begins to drop at 15 January and reaches minimum on 24 January. The F2

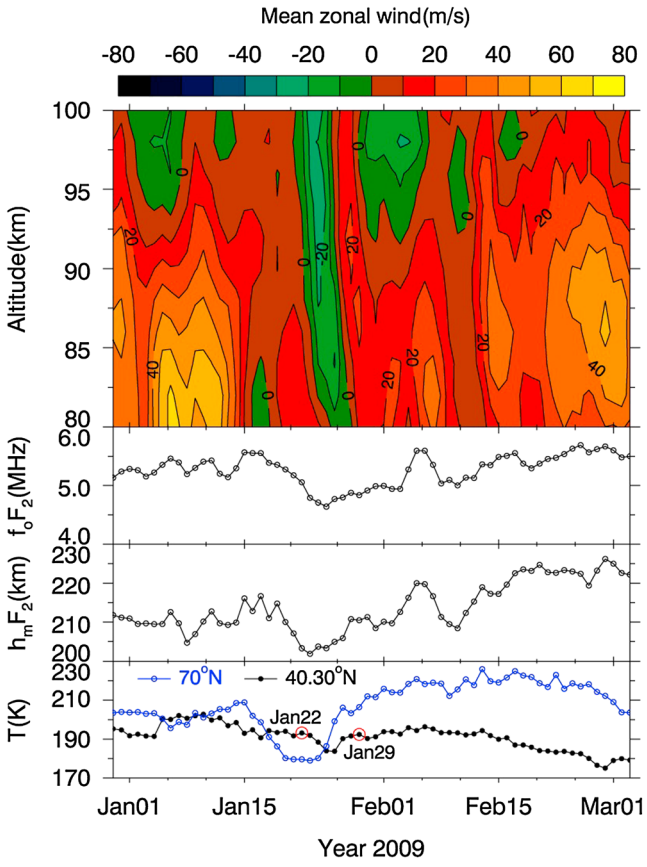

Figure 2. The first panel is the mean zonal wind observed by the meteor radar. The second and third panels are *F*2 layer critical frequency f_oF_2 and F2 peak height h_mF_2 averaged from 12 to 16 local times. Zonal mean temperatures at about 88 km observed by Aura at 2.3 LT at 40.30°N and 70°N are shown in the fourth panel.

peak height h_mF_2 drops during 15 and 24 January. On 24 January, f_oF_2 has diminished about 1 MHz, and h_mF_2 has dropped 10 km compared with those on 15 January. According to the global observation of COSMIC satellites, the averaged h_mF_2 dropped about 19 km [*Yue et al.*, 2010]. The echoes of CADI in the morning are so weak that we cannot obtain reliable parameters from the ionogram. The TEC over Beijing will be checked to investigate the variation of ionosphere with local time.

[13] Figure 3 shows the mean TEC from 1 January to 10 January and the difference between TEC observations and the mean TEC. The mean TEC represents quiet time TEC reference. From 15 January to 21 January, the perturbation of TEC exhibits diurnal variation. Between 22 and 27 January, the perturbation of TEC shows significant semidiurnal variation. There is a TEC peak in the morning and then shifts to later local time in next day as indicated by the dashed line in the middle panel of Figure 3. The perturbation of TEC also shows semidiurnal variation in the morning from 28 January to 3 February but without peak shifting. It seems the TEC perturbation is a combination of diurnal, semidiurnal, and terdiurnal variations during this period. We will analyze those variations later. There is an increased geomagnetic activity after 3 February; the TEC has large deviation from the reference in February.

3.2. Tidal Variation of Winds in the Mesosphere and TEC in the Ionosphere

[14] To study variation of winds in the mesosphere and TEC in the ionosphere, we apply a harmonic analysis to the meteor radar wind from 80–100 km and to perturbation TEC. Dominant solar tides are diurnal, semidiurnal, and terdiurnal with periods 24 h, 12 h, and 8 h, respectively. The semidiurnal lunar tide with period at about 12.42 h is the dominant lunar tide. Winds and TEC are assumed to consist of the above components, as can be seen from the following equation [*Malin and Schlapp*, 1980]:

$$U = U_0 + A_1\cos\left(\frac{2\pi}{24}t + \varphi_1\right) + A_2\cos\left(\frac{2\pi}{12}t + \varphi_2\right)A_3\cos\left(\frac{2\pi}{8}t + \varphi_3\right) + A_4\cos\left(\frac{2\pi}{12}t + \varphi_4\right) \quad (1)$$

where t is the solar time and τ is the lunar time; $\tau = t - v$, and v is the lunar age, which is equal to 0 at the new moon and 180 at the full moon in angular measurement. The solar diurnal, semidiurnal, and terdiurnal tides and the semidiurnal lunar tides have amplitudes A_1, A_2, A_3, A_4 and phases $\varphi_1, \varphi_2, \varphi_3, \varphi_4$. Generally, tidal phase means the local time (solar or lunar) when the tide reaches its maximum. As the periods of solar and semidiurnal lunar tides are close, the length of the data set should be at least 14.78 days to provide the spectral resolution to separate the solar and lunar components. We perform the harmonic analysis with window length 15 days, shifting 1 day. It has been proven that solar and lunar tides can be obtained using the above method [*Niu et al.*, 2005; *Paulino et al.*, 2012].

[15] We perform the harmonic analysis to the TEC perturbation which is the difference between observations and mean TEC. Figure 4 represents solar and lunar amplitudes and phases of TEC during January and February 2009. As the diurnal variation of ionosphere is so strong, the TEC perturbation may still contain some diurnal variation of TEC background, especially at time far away from the days for mean TEC computation. The monotonic amplitude of diurnal component in perturbation TEC may include contribution from seasonal variation of ionosphere and diurnal atmospheric tide. The semidiurnal and terdiurnal components increase after 18 January. The phase of semidiurnal component tends to shift early after the onset of SSW. The semidiurnal lunar tides are shown in Figures 4g and 4h. Comparing with solar tides, the semidiurnal lunar tide is the one that gets amplified the most after the onset of the SSW. Lunar tide reaches its maximum at time shift to later local time with the progress of days as shown in Figure 4h. The lunar tide has comparable or even larger amplitude than the solar semidiurnal tide during 22 to 27 January. The combination of lunar and solar semidiurnal tides in TEC contributes to the semidiurnal variation in TEC, and its peak shifts consistently to later local time as shown in the middle panel of Figure 3.

[16] Next, we will check wind variation in the mesosphere. Figure 5 shows the amplitude of solar and lunar tides in the zonal wind in the mesosphere. Figure 6 shows the amplitudes of tides in the meridional wind. The main characteristic are as follows. (1) The solar diurnal tides in zonal and meridional

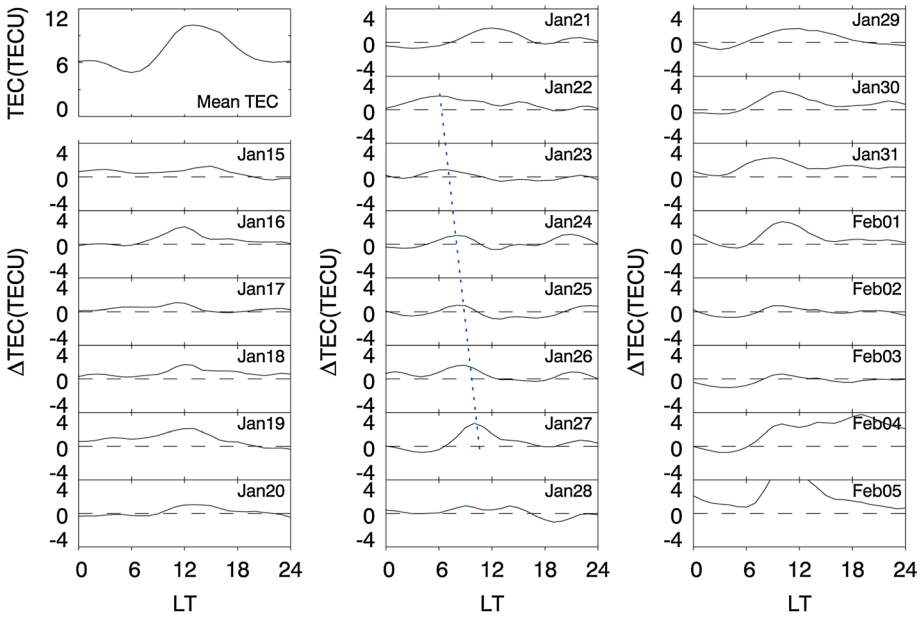

Figure 3. TEC variation over Beijing. The left upper panel is the mean TEC during 1 and 10 January. Δ TEC is the TEC perturbation, i.e., the difference between TEC observation and the mean TEC. The TEC variations from 20 January to 5 February are shown in the figure from left to right panels. The blue dotted line indicates the maximum in the morning from 22 to 27 January.

wind increase at the end of January a few days after the onset of SSW. The amplitudes of both zonal and meridional components reach their maximum at 92 km in the middle of February. (2) The amplitude of terdiurnal solar tide is very small, but a small enhancement in meridional amplitude can also be found between 1 to 15 February as shown in Figure 6b. (3) During 1 January to 1 March, the semidiurnal solar tide in zonal and meridional wind shows large variations. The amplitude of semidiurnal solar tide begins to increase before 1 January and reaches its maximum around 2 January. Then the zonal amplitude decreases rapidly from about 18 m/s to 8 m/s at 22 January just around the zonal wind reversal day. The meridional amplitude shows similar variation. After 22 January, semidiurnal tide increases again and shows variation with period of about 16–20 days above 90 km. (4) Before 15 January, the semidiurnal lunar tide is very weak. It begins to increase obviously from 15 January and reaches maximum at about 2 February. Then the amplitude decays rapidly to small value after middle of February. The maximum amplitude, 15 m/s for zonal wind and 21 m/s for meridional wind, appears at about 96 km. The amplitude also has oscillation with several days before decay. In this study, the length of moving fit window with formula (1) is 15 days, which is less than most of similar studies. Window length 15 days is long enough to distinguish the solar and semidiurnal lunar tides theoretically, although the risk of aliasing into each other increases. If a long window is adopted, the amplitudes of tides may reduce, important time points may change, and the oscillation of amplitude cannot be seen. Recently, a fit

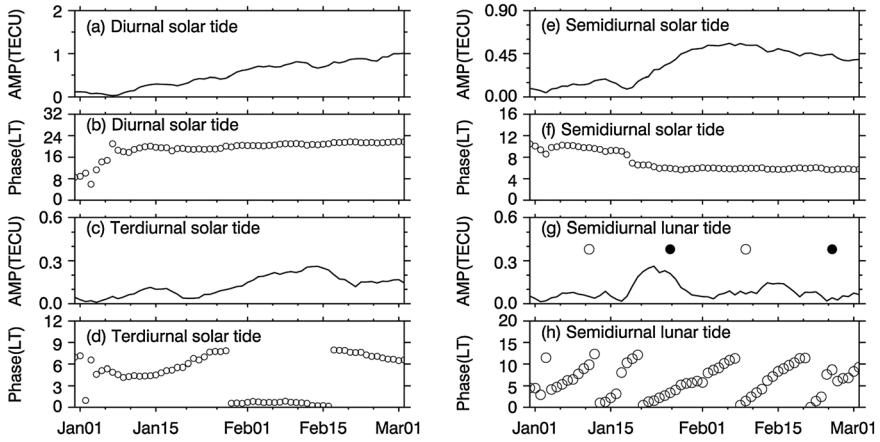

Figure 4. Tidal components in perturbation TEC. (a, c, e, and g) Amplitudes. (b, d, f, and h) Phases. The lunar phase also shows solar local time. The open circles and solid circles in Figure 4g represent full and new moons.

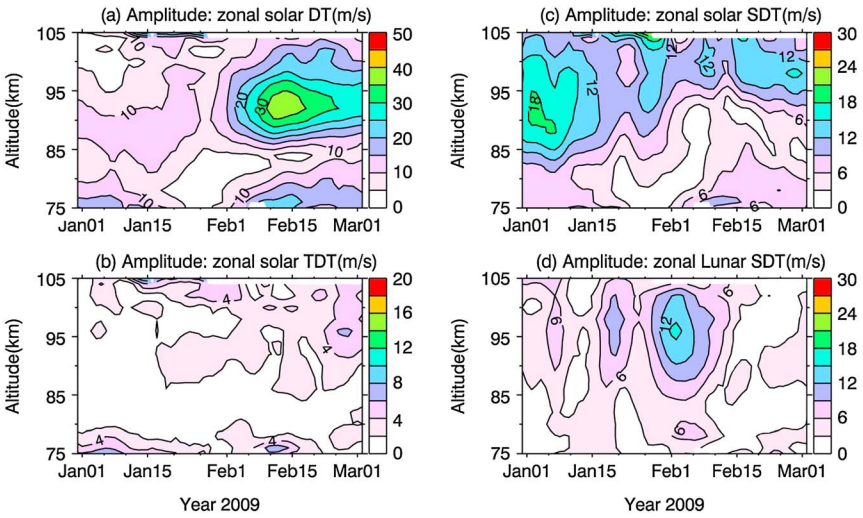

Figure 5. Amplitudes of solar and lunar tides in the zonal wind over Beijing. (a) Diurnal solar tide. (b) Terdiurnal solar tide. (c) Semidiurnal solar tide. (d) Semidiurnal lunar tide.

within a moving window with 16 days is adopted to study tides in low latitude [*Sathishkumar and Sridharan*, 2013]. Their results also show oscillations in tidal amplitudes.

[17] All tidal amplitudes change before and after SSW. But the most significant feature is the variability of both semidiurnal solar and semidiurnal lunar tides. Semidiurnal solar tide is produced mainly due to solar insolation absorption of ozone in the stratosphere. The variation in the stratosphere could change the ozone mixing and its global distribution because of the changing meridional circulation during SSW [*Sridharan et al*., 2012]. The strong activity of planetary waves [*Pancheva et al*., 2008] during SSW could also alter the distribution of ozone [*Goncharenko et al*., 2012]. The semidiurnal solar tide may change with its source variation and be modified by the nonlinear interaction with planetary waves [*Liu et al*., 2010]. We can see semidiurnal solar tide variation and planetary type oscillation during January and February from Figure 5c and 6c. The increase of solar semidiurnal tide at 96 km begins at middle of December in 2008 (not shown here), and the oscillation persists during SSW. The amplitude decays before SSW from 1 January. Although there is not any significant maximum below 100 km during SSW, it seems that the tidal amplitude has a tendency to increase above 105 km from Figures 5c and 6c, which is consistent with the numerical result. The numerical simulations show that the maximum of semidiurnal solar tide is between 110 km and 120 km, which is generally out of meteor radar wind range [*Jin et al*., 2012; *Pedatella et al*., 2012; *Du et al*., 2007]. The SSW in 2009 mainly results from intense amplification of planetary wave 2 (PW2) in January 2009. But planetary wave 1 (PW1) is very large [*Goncharenko et al*., 2010b] during December 2008 and at the beginning of 2009. Although the abruption of PW2 induces the SSW in 2009, the maximum of PW1 in December 2008 is even stronger than the maximum of PW2 during SSW [*Goncharenko et al*., 2010b]. The nonlinear interaction between PW1 and migrating semidiurnal tide SW2 may

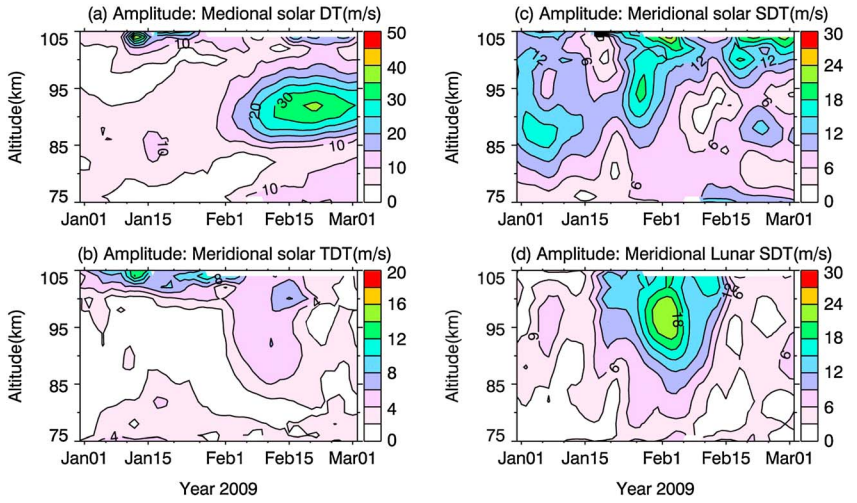

Figure 6. Same as Figure 5 but for the meridional wind.

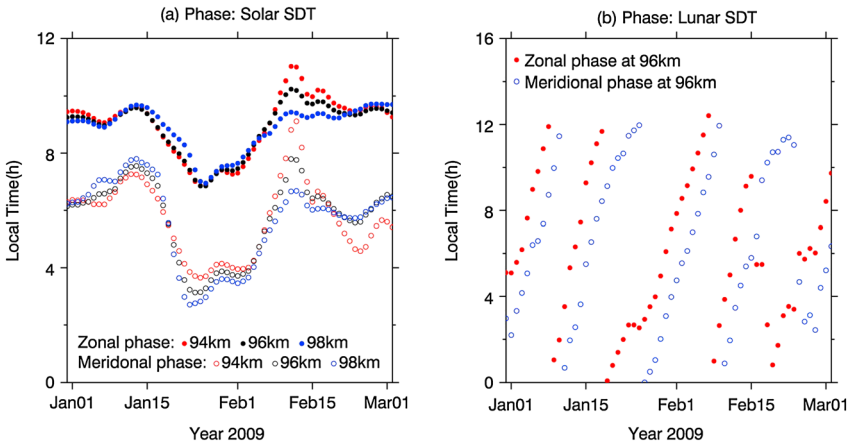

Figure 7. Phases of semidiurnal tides. (a) Phases of semidiurnal solar tide at 94, 96, and 98 km. (b) Phases of lunar semidiurnal tide at 96 km.

generate nonmigrating semidiurnal SW1 and SW3. Then the observed value of semidiurnal tide, which is the sum of SW2 and nonmigrating tides, could increase when PW1 is strong. The large amplitude of solar semidiurnal tide till the beginning of 2009 may be the result of nonlinear interaction between PW1 and SW2. As the impact of PW1 on midlatitude is much larger than on low latitude, the increase of semidiurnal tide at low latitude cannot be seen during December in 2008 and at beginning of 2009 [*Sridharan et al*., 2012].

[18] As shown in Figures 5d and 6d, the amplitude of semidiurnal lunar tide is the same as or even a little larger than the amplitude of solar semidiurnal tides during SSW. The GSWM (Global Scale Wave Model) has been used to simulate variation of lunar tide. *Stening et al.* [1997] proposed that the wind structure during SSW is beneficial for the growing lunar tide. *Forbes and Zhang* [2012] explained why the wind structure during SSW can help the lunar tide to increase using the same GSWM model. A normal mode named Pekeris peak with period at about 12.81 h shifts to a small period during the SSW. When the period shifts close enough to the period of semidiurnal lunar tide, resonance will happen between the normal mode and semidiurnal lunar tide. The semidiurnal lunar tide could increase rapidly. The results of simulation show that the enhancements in the migrating semidiurnal lunar tide is larger than in the migrating semidiurnal solar tide [*Pedatella et al*., 2012] at midlatitudes to high latitudes, which is consistent with the observations as shown in Figures 5 and 6. The observation of SABER shows the semidiurnal lunar tides maximize near day 35 of 2009 [*Forbes and Zhang*, 2012], which is very close to 2 February when zonal and meridional lunar semidiurnal tides reach their maxima in Beijing. According to the transient tidal propagation experiments [*Vial et al*., 1991], *Forbes and Zhang* [2012] proposed that there were 7–8 days delay between forcing and response for the first symmetric semidiurnal tidal mode. Then the maximum semidiurnal lunar tide could be forced on about 25–26 January around new moon day, when the lunar phase is around 0°. The gravitational force could generate large tide in the new moon day. So it is reasonable that the lunar tide in the mesosphere appears at 2 February. The significant enhancement of semidiurnal lunar tide is from 15 January to 15 February, which is also consistent with SABER observation. Results from model simulation show the maximum of wind semidiurnal lunar tide is around latitude 40° [*Forbes and Zhang*, 2012; *Pedatella et al*., 2012]. Beijing is located at 40.30°N, and the amplitudes of lunar winds over Beijing are 15 to 21 m/s at 96 km during the SSW. The global largest amplitudes of semidiurnal lunar tide in winds at about 96 km may be approximately 15 to 21 m/s, which is a little smaller than the amplitude of about 30 m/s by GSWM [*Forbes and Zhang*, 2012].

[19] Figure 7 shows the phase variation of semidiurnal solar and lunar tides of wind. Figure 7a represents phases of solar tide at 94, 96, and 98 km. The solid circles are for zonal wind, and open circles are for meridional wind. The phases at different altitudes are very close to each other. That means the vertical wavelength of solar semidiurnal tide is quite large. The tidal phase in meridional wind is 2–6 h lead to that in zonal wind as many other observations [*Sathishkumar and Sridharan*, 2013]. From 15 January, the phase of both zonal and meridional tides drop 3–4 h and then recover at about 10 February. This type of tidal phase variation is somewhat like the tidal phase variation from winter to summer and then to winter. In many observations, the phases of solar diurnal and semidiurnal tides in the mesopause reach maxima in winter months when it is warm and reach minima in summer months when it is cold [*Xiong et al*., 2004; *Yuan et al*., 2008], possibly related to the variation of Hough mode. The mesopause becomes cold before SSW and then returns to warm after SSW, which is quite similar to the temperature variation from winter to summer and again to winter in the mesosphere. The ozone variation [*Goncharenko et al*., 2012] may also change the mode during SSW. That means ozone variation during SSW may lead to the variation of semidiurnal solar tide in the stratosphere and in the mesosphere in turn. But the situation may be complex. The observation in low latitude does not show such significant phase variation in solar semidiurnal tide. The variation of phases of semidiurnal solar tide in zonal and meridional wind is not the same before and after SSW [*Sathishkumar and Sridharan*,

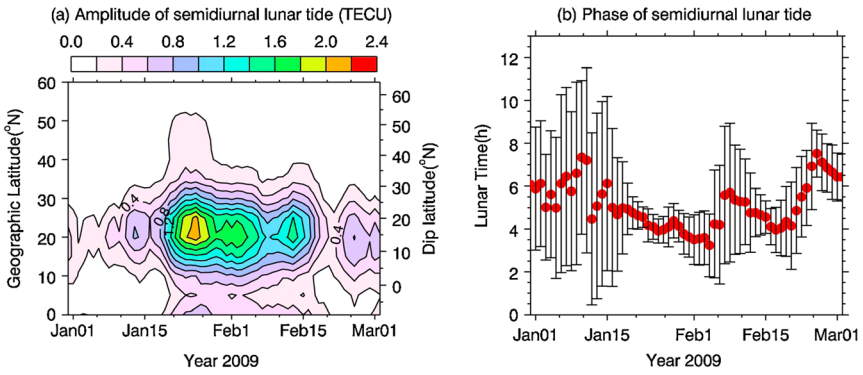

Figure 8. Amplitude and phase of semidiurnal lunar tide in IGS-TEC perturbation along 120°E in the Northern Hemisphere. (a) Amplitude. (b) Average phase from geographic equator to 60°N. Error bars are standard deviations.

2013]. Figure 7b shows the phase variation of semidiurnal lunar tide at 96 km. The meridional component leads 2–4 h to the zonal component. As we have mentioned, semidiurnal lunar tide reaches maximum on 2 February. At this time, the phases of zonal and meridional component are 5.5 and 8.5 solar local time, which are close to the SABER observation [*Forbes and Zhang*, 2012]. The phase variation of semidiurnal lunar tide can also be seen in the low latitudes [*Sathishkumar and Sridharan*, 2013].

4. Discussion

[20] The response of ionosphere to the SSW with phase shift is remarkable in the low latitudes [*Chau et al.*, 2010; *Fejer et al.*, 2010; *Liu et al.*, 2011]. But the amplitude of semidiurnal lunar tide in TEC is very small in Beijing shown in Figure 4g. In order to check if the enhancement of lunar tide is a global feature, we do the same harmonic fit for the IGS-TEC along longitude 120°E in the Northern Hemisphere. The solar tides have been studied using the IGS-TEC and show variation during 2009 SSW [*Pedatella and Forbes*, 2010]. Figure 8a represents the amplitude of semidiurnal lunar tide with day and latitude. The strongest response appears at about geographic latitude 15–20°N or dip latitude 15°N in the equatorial ionospheric anomaly (EIA) crest. In midlatitude and high latitude, the lunar tide is much weaker than in the fountain region, and the enhancement range is limited before 1 February that is a few days after the peak SSW. The significant lunar tide in low latitude persists for more about 1 month, but it exists for only about 10 days in the midlatitudes. The TEC perturbation caused by the geomagnetic disturbances in February may diminish the relative perturbation in lunar tide in the midlatitudes. The observation of TEC in Beijing shows a similar result as shown in Figure 4d. Figure 8b represents the variation of average phase of semidiurnal lunar tide. The phases in Figures 8b and 9b are in local lunar time. It is better to represent phases of lunar tide in local lunar time when lunar tides are compared. We have known that if the amplitude of tide is small, the phase determination is not so reliable [*Stening et al.*, 1994]. The relative small amplitude before 15 January and after 5 February is responsible for large phase bias. The geomagnetic disturbance in February could affect the phase estimation especially when the tide is weak. But when the tide has large amplitude during 15 January to 2 February, the average phase is at about 4:00 local lunar time with standard deviation less than 2 h. From the small bias, it could be inferred that the

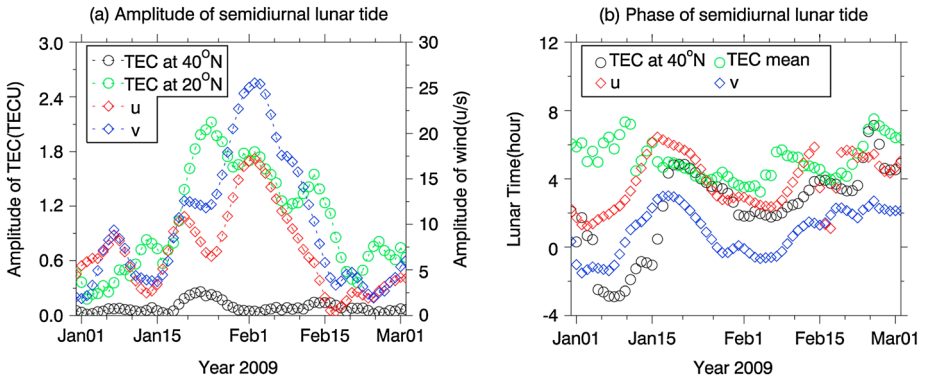

Figure 9. Amplitudes and phases of semidiurnal lunar tides in wind and TEC. (a) Amplitude. Open circles represent the amplitude of semidiurnal lunar tide in TEC. Open diamonds represent the amplitude of semidiurnal lunar tide in wind at 96 km. The amplitude for TEC at 40°N is from observation and at 20°N is from IGS-TEC. (b) Phase. The phase of TEC at 40°N is from observation. The phase labeled with TEC mean is the averaged phase in the Northern Hemisphere.

semidiurnal lunar tide along the longitude is generated from the same source. We will then compare variation of semidiurnal lunar tide in TEC and wind to see if they are correlated to each other.

[21] Figure 9a represents the amplitudes of lunar tide from observation. The amplitude of TEC at 20°N from IGS-TEC is also shown in the figure. All of the lunar tidal amplitudes of zonal wind, meridional wind, and TEC perturbation at 20°N are enhanced during 15 January and 15 February. The lunar tide in the EEJ in low-latitude ionosphere enhances during the similar period as shown by [*Sathishkumar and Sridharan*, 2013]. Comparing with the lunar tide in the low latitude, the lunar tide in wind is much stronger but with very similar variation during SSW. Figure 9b represents the phase of TEC and winds in lunar time. The mean TEC phase along the longitude 120°E in the Northern Hemisphere is also shown in Figure 9b. The phase of meridional wind leads about 3–4 lunar hours to zonal wind. The phases of all quantities change during SSW.

[22] From the comparison of the phase of the observed TEC, zonal wind at 96 km, the semidiurnal variation in TEC and zonal wind are almost in phase, especially at the end of January when they are strong. There are at least two mechanisms which can couple mesosphere and ionosphere through tides. One is that the tide propagates to ionospheric *F* region directly and drives the ionosphere and makes TEC variation. In this case, the phase of TEC (which is mainly related to ionosphere peak at about 300–400 km) may not have a good relationship with the phase in the mesosphere because the tides propagate about more than 200 km vertically through variable atmosphere. The other mechanism is the electrodynamic coupling in the dynamo region at about 110–140 km. According to the ionospheric dynamo theory, the lunar tide in the ionospheric *E* layer could affect the dynamo and modulate the ionospheric electric field in the *E* layer. This electric field can map into the *F* region along the magnetic field lines. Then the disturbance in the *E* layer can be seen in the *F* layer especially at EIA crests because of the fountain amplification effects. From Figure 9b, the phases of zonal wind and mean TEC are very close to each other during SSW. This feature seems to imply that the global semidiurnal lunar tide in TEC is correlated with the lunar component in zonal wind. A comparison between winds over Wuhan and Adelaide in the Northern and Southern Hemispheres shows that the semidiurnal lunar tide is symmetric in January [*Niu et al*., 2005]. *Stening et al*. [2003] also indicated that the semidiurnal lunar tide is dominated by the Hough mode symmetric (2, 2) below and above 120 km. So the zonal tidal winds in the two hemispheres are in phase in the dynamo region. Then the associated dynamo electric field $\mathbf{U} \times \mathbf{B}$ and balanced polarized electric field must be in the same direction. That means the electric field in the *F* region mapped from *E* layer is also symmetric to the equator. The zonal component of electric fields from different hemisphere should be in the same direction and the electric field in the equator could be superposed in the *F* layer. But for the antisymmetric meridional wind mode (2, 2), the zonal electric fields from different hemispheres are in opposite directions. The *F* electric field mapped from the *E* layer could be eliminated in the equator. So the lunar tide of zonal wind is responsible for the global semidiurnal lunar tide in the *F* layer. That is the reason why semidiurnal tides in TEC and zonal wind are in phase. It is the same as the correlation between ionosphere wave number 4 structures and nonmigrating tide in the mesosphere [*Wan et al*., 2010]. Over Beijing, the electric field generated by meridional wind could also be decreased or be eliminated by antisymmetric electric field from the conjugate point. Meanwhile, the electric field generated by zonal wind could be strengthened. That makes the in-phase variation of lunar tides in TEC and zonal wind over Beijing. So the coupling between mesosphere and ionosphere through lunar tide is from electrodynamics in the dynamo region during the SSW. When the lunar tide is small, there is no coupling between mesosphere and ionosphere through lunar tide, and no relationship can be found in the phases of lunar tide in TEC and wind.

[23] The phase of semidiurnal solar tide increases from about 3 to 10 February when the tide recovers to the normal state before SSW as shown in Figure 7a. During this period, the semidiurnal solar tide of wind is quite strong. If the semidiurnal solar tide deduces a response in the ionosphere, the generated solar semidiurnal tide could have phase shift forward. So it seems to be possible for TEC to shift its maximum forward during SSW without enhancement of lunar tide over Beijing. But it is not true in the 2009 SSW from our observation during 3 and 10 February. So we can conclude that the semidiurnal variation of TEC is the result of enhancement of both solar and semidiurnal lunar tides in the mesosphere, and the enhancement of semidiurnal lunar tides is responsible for the peak shift forward in TEC during SSW.

5. Conclusion

[24] Based on wind observations by a meteor radar and TEC by a TEC receiver in Beijing (40.6°N, 116.19°E geographic, 39.73°N dip latitude), the response of middle atmosphere and ionosphere over Beijing has been studied. In the mesosphere, eastward mean zonal wind decreases before the onset of SSW at 10 hPa and reverse to westward during 21 to 27 February just around the peak SSW at 10 hPa, first at 100 km and then downward to 80 km. The critical frequency of F2 layer (f_oF_2) and peak height (h_mF_2) in the ionosphere decreased 1 MHz and 8 km during the SSW in the afternoon.

[25] We focus on finding the reason of enhancement of semidiurnal variation with maximum shift forward in TEC perturbation during 22 to 27 January. The wind and TEC are decomposed to solar and lunar tide. During SSW, the diurnal and terdiurnal solar tides increase both in the wind and TEC. The most significant variation is the enhancement of semidiurnal solar and lunar tides. The oscillation with period at about 16–20 days can be seen in the tidal amplitudes. The PW1 which increases in middle of December 2008 and decays at beginning of January 2009 and PW2 which is large in January could make the solar semidiurnal tides increase during December 2008 and January 2009 through nonlinear interaction. We can also see the phase variation of solar tides during SSW.

[26] The enhancement in semidiurnal lunar tide in TEC can be seen from 17 January to 2 February. During those days; semidiurnal lunar tide in wind is also quite large. The maximum amplitudes of zonal and meridional lunar

tide reach about 15 m/s and 21 m/s at about 96 km. The enhancement of TEC lunar tide can be seen in the low latitude with maximum in the EIA crest in the similar days. That indicates the enhancement in lunar tides in mesosphere induced the enhancement in TEC. We also compare the phase variation of lunar tide in TEC and wind. During SSW when the lunar tide is large, lunar tides in zonal wind and TEC reach their maximum at the similar time which is about 2 to 4 lunar hours lag behind the meridional wind. The result is corresponding to the ionospheric dynamo theory, as the dominant Hough mode of lunar tides is the symmetric mode (2,2) above 120 km. We conclude the semidiurnal variation of TEC results from enhancement in both solar and semidiurnal lunar tides in the mesosphere, and the enhancement in semidiurnal lunar tides is responsible for the peak shift forward during SSW.

[27] **Acknowledgments.** This work is supported by the National Science Foundation of China (40974086) and National Important basic Research Project of China (2011CB811405). Thanks to National Center for Environment Prediction and the MLS/AURA Team for the use of related data. We also thank IGS for making available TEC data.

[28] Robert Lysak thanks the reviewers for their assistance in evaluating this paper.

References

Anderson, D., and E. Araujo-Pradere (2010), Sudden stratospheric warming event signatures in daytime E×B drift velocities in the Peruvian and Philippine longitude sectors for January 2003 and 2004, *J. Geophys. Res.*, *115*, A00G05, doi:10.1029/2010JA015337.

Chau, J. L., B. G. Fejer, and L. P. Goncharenko (2009), Quiet variability of equatorial E×B drifts during a sudden stratospheric warming event, *Geophys. Res. Lett.*, *36*, L05101, doi:10.1029/2008GL036785.

Chau, J. L., N. A. Aponte, E. Cabassa, M. P. Sulzer, L. P. Goncharenko, and S. A. Gonzalez (2010), Quiet time ionospheric variability over Arecibo during sudden stratospheric warming events, *J. Geophys. Res.*, *115*, A00G06, doi:10.1029/2010JA015378.

Chau, J. L., L. P. Goncharenko, B. G. Fejer, and H.-L. Liu (2011), Equatorial and low latitude ionospheric effects during sudden stratospheric warming events, *Space Sci. Rev.*, *168*(1–4), 385–417, doi:10.1007/s11214-011-9797-5.

Ding, F., W. Wan, B. Ning, B. Zhao, Q. Li, R. Zhang, B. Xiong, and Q. Song (2012), Two-dimensional imaging of large-scale traveling ionospheric disturbances over China based on GPS data, *J. Geophys. Res.*, *117*, A08318, doi:10.1029/2012JA017546.

Du, J., W. Ward, J. Oberheide, T. Nakamura, and T. Tsuda (2007), Semidiurnal tides from the extended Canadian Middle Atmosphere Model (CMAM) and comparisons with TIMED Doppler interferometer (TIDI) and meteor radar observations, *J. Atmos.Sol. Terr. Phys.*, *69*(17–18), 2159–2202, doi:10.1016/j.jastp.2007.07.014.

Fang, T. W., T. Fuller-Rowell, R. Akmaev, F. Wu, H. Wang, and D. Anderson (2012), Longitudinal variation of ionospheric vertical drifts during the 2009 sudden stratospheric warming, *J. Geophys. Res.*, *117*, A03324, doi:10.1029/2011JA017348.

Fejer, B. G., M. E. Olson, J. L. Chau, C. Stolle, H. Lühr, L. P. Goncharenko, K. Yumoto, and T. Nagatsuma (2010), Lunar-dependent equatorial ionospheric electrodynamic effects during sudden stratospheric warmings, *J. Geophys. Res.*, *115*, A00G03, doi:10.1029/2010JA015273.

Forbes, J. M., and X. Zhang (2012), Lunar tide amplification during the January 2009 stratosphere warming event: Observations and theory, *J. Geophys. Res.*, *117*, A12312, doi:10.1029/2012JA017963.

Fuller-Rowell, T., F. Wu, R. Akmaev, T.-W. Fang, and E. Araujo-Pradere (2010), A whole atmosphere model simulation of the impact of a sudden stratospheric warming on thermosphere dynamics and electrodynamics, *J. Geophys. Res.*, *115*, A00G08, doi:10.1029/2010JA015524.

Fuller-Rowell, T., H. Wang, R. Akmaev, F. Wu, T.-W. Fang, M. Iredell, and A. Richmond (2011), Forecasting the dynamic and electrodynamic response to the January 2009 sudden stratospheric warming, *Geophys. Res. Lett.*, *38*, L13102, doi:10.1029/2011GL047732.

Gao, H., J. Xu, W. Ward, and A. K. Smith (2011), Temporal evolution of nightglow emission responses to SSW events observed by TIMED/SABER, *J. Geophys. Res.*, *116*, D19110, doi:10.1029/2011JD015936.

Goncharenko, L. P., and S.-R. Zhang (2008), Ionospheric signatures of sudden stratospheric warming: Ion temperature at middle latitude, *Geophys. Res. Lett.*, *35*, L21103, doi:10.1029/2008GL035684.

Goncharenko, L. P., J. L. Chau, H. L. Liu, and A. J. Coster (2010a), Unexpected connections between the stratosphere and ionosphere, *Geophys. Res. Lett.*, *37*, L10101, doi:10.1029/2010GL043125.

Goncharenko, L. P., A. J. Coster, J. L. Chau, and C. E. Valladares (2010b), Impact of sudden stratospheric warmings on equatorial ionization anomaly, *J. Geophys. Res.*, *115*, A00G07, doi:10.1029/2010JA015400.

Goncharenko, L., A. Coster, R. Plumb, and D. Domeisen (2012), The potential role of stratospheric ozone in the stratosphere-ionosphere coupling during stratospheric warmings, *Geophys. Res. Lett.*, *39*, L08101, doi:10.1029/2012GL051261.

Harada, Y., A. Goto, H. Hasegawa, N. Fujikawa, H. Naoe, and T. Hirooka (2010), A major stratospheric sudden warming event in January 2009, *J. Atmos. Sci.*, *67*(6), 2052–2069, doi:10.1175/2009jas3320.1.

Hoffmann, P., W. Singer, D. Keuer, W. Hocking, M. Kunze, and Y. Murayama (2007), Latitudinal and longitudinal variability of mesospheric winds and temperatures during stratospheric warming events, *J. Atmos. Sol. Terr. Phys.*, *69*(17–18), 2355–2366, doi:10.1016/j.jastp.2007.06.010.

Jin, H., Y. Miyoshi, D. Pancheva, P. Mukhtarov, H. Fujiwara, and H. Shinagawa (2012), Response of migrating tides to the stratospheric sudden warming in 2009 and their effects on the ionosphere studied by a whole atmosphere-ionosphere model GAIA with COSMIC and TIMED/SABER observations, *J. Geophys. Res.*, *117*, A10323, doi:10.1029/2012JA017650.

Kurihara, J., Y. Ogawa, S. Oyama, S. Nozawa, M. Tsutsumi, C. M. Hall, Y. Tomikawa, and R. Fujii (2010), Links between a stratospheric sudden warming and thermal structures and dynamics in the high-latitude mesosphere, lower thermosphere, and ionosphere, *Geophys. Res. Lett.*, *37*, L13806, doi:10.1029/2010GL043643.

Lasvtovilcvka, J., and B. A. de la Morena (1987), The response of the lower ionosphere in central and southern Europe to anomalous stratospheric conditions, *Phys. Scripta*, *35*(6), 902.

Lin, J. T., C. H. Lin, L. C. Chang, H. H. Huang, J. Y. Liu, A. B. Chen, C. H. Chen, and C. H. Liu (2012), Observational evidence of ionospheric migrating tide modification during the 2009 stratospheric sudden warming, *Geophys. Res. Lett.*, *39*, L02101, doi:10.1029/2011GL050248.

Liu, H. L., and R. G. Roble (2002), A study of a self-generated stratospheric sudden warming and its mesospheric–lower thermospheric impacts using the coupled TIME-GCM/CCM3, *J. Geophys. Res.*, *107*(D23), 4695, doi:10.1029/2001JD001533.

Liu, H. L., W. Wang, A. D. Richmond, and R. G. Roble (2010), Ionospheric variability due to planetary waves and tides for solar minimum conditions, *J. Geophys. Res.*, *115*, A00G01, doi:10.1029/2009JA015188.

Liu, H., M. Yamamoto, S. Tulasi Ram, T. Tsugawa, Y. Otsuka, C. Stolle, E. Doornbos, K. Yumoto, and T. Nagatsuma (2011), Equatorial electrodynamics and neutral background in the Asian sector during the 2009 stratospheric sudden warming, *J. Geophys. Res.*, *116*, A08308, doi:10.1029/2011JA016607.

Malin, S. R. C., and D. M. Schlapp (1980), Geomagnetic lunar analysis by least-squares, *Geophys. J. R. Astr. Soc.*, *60*, 409–418.

Manney, G. L., M. J. Schwartz, K. Krüger, M. L. Santee, S. Pawson, J. N. Lee, W. H. Daffer, R. A. Fuller, and N. J. Livesey (2009), Aura Microwave Limb Sounder observations of dynamics and transport during the record-breaking 2009 Arctic stratospheric major warming, *Geophys. Res. Lett.*, *36*, L12815, doi:10.1029/2009GL038586.

Matsuno, T. (1971), A dynamical model of the stratospheric sudden warming, *J. Atmos. Sci.*, *28*(8), 1479–1494.

Niu, X., J. Xiong, W. Wan, B. Ning, L. Liu, R. A. Vincent, and I. M. Reid (2005), Lunar tidal winds in the mesosphere over Wuhan and Adelaide, *Adv. Space Res.*, *36*(11), 2218–2222.

Pancheva, D., et al. (2008), Planetary waves in coupling the stratosphere and mesosphere during the major stratospheric warming in 2003/2004, *J. Geophys. Res.*, *113*, D12105, doi:10.1029/2007JD009011.

Paulino, A. R., P. P. Batista, B. R. Clemesha, R. A. Buriti, and N. Schuch (2012), An enhancement of the lunar tide in the MLT region observed in the Brazilian sector during 2006 SSW, *J. Atmos. Sol. Terr. Phys.*, *90–91*, 97–103, doi:10.1016/j.jastp.2011.12.015.

Pedatella, N. M., and J. M. Forbes (2010), Evidence for stratosphere sudden warming-ionosphere coupling due to vertically propagating tides, *Geophys. Res. Lett.*, *37*, L11104, doi:10.1029/2010GL043560.

Pedatella, N. M., H. L. Liu, A. D. Richmond, A. Maute, and T. W. Fang (2012), Simulations of solar and lunar tidal variability in the mesosphere and lower thermosphere during sudden stratosphere warmings and their influence on the low-latitude ionosphere, *J. Geophys. Res.*, *117*, A08326, doi:10.1029/2012JA017858.

Sathishkumar, S., and S. Sridharan (2013), Lunar and solar tidal variabilities in mesospheric winds and EEJ strength over Tiruneveli (8.7°N, 77.8°E)

during the 2009 major stratospheric warming, *J. Geophys. Res.*, *118*, doi:10.1029/2012JA018236.

Sathishkumar, S., S. Sridharan, and C. Jacobi (2009), Dynamical response of low-latitude middle atmosphere to major sudden stratospheric warming events, *J. Atmos. Sol. Terr. Phys.*, *71*(8–9), 857–865, doi:10.1016/j.jastp.2009.04.002.

Shepherd, M. G., D. Wu, I. Fedulina, S. Gurubaran, J. Russell, M. Mlynczak, and G. Shepherd (2007), Stratospheric warming effects on the tropical mesospheric temperature field, *J. Atmos. Sol. Terr. Phys.*, *69*(17–18), 2309–2337, doi:10.1016/j.jastp.2007.04.009.

Sridharan, S., S. Sathishkumar, and S. Gurubaran (2009), Variabilities of mesospheric tides and equatorial electrojet strength during major stratospheric warming events, *Ann. Geophys.*, *27*, 4125–4130.

Sridharan, S., K. Raghunath, S. Sathishkumar, and D. Nath (2010), First results of warm mesospheric temperature over Gadanki (13.5 degrees N, 79.2 degrees E) during the sudden stratospheric warming of 2009, *J. Atmos. Sol. Terr. Phys.*, *72*(14–15), 1139–1146, doi:10.1016/j.jastp.2010.06.003.

Sridharan, S., S. Sathishkumar, and S. Gurubaran (2012), Variabilities of mesospheric tides during sudden stratospheric warming events of 2006 and 2009 and their relationship with ozone and water vapour, *J. Atmos. Sol. Terr. Phys.*, *78–79*, 108–115, doi:10.1016/j.jastp.2011.03.013.

Stening, R. J. (2011), Lunar tide in the equatorial electrojet in relation to stratospheric warmings, *J. Geophys. Res.*, *116*, A12315, doi:10.1029/2011JA017047.

Stening, R. J., A. H. Manson, C. E. Meek, and R. A. Vincent (1994), Lunar tidal winds at Adelaide and Saskatoon at 80 to 100 km heights: 1985–1990, *J. Geophys. Res.*, *99*(A7), 13,273–13,280.

Stening, R. J., J. M. Forbes, M. E. Hagan, and A. D. Richmond (1997), Experiments with a lunar atmospheric tidal model, *J. Geophys. Res.*, *102*(D12), 13,465–13,471.

Stening, R. J., T. Tusda, T. Nakamura (2003), Lunar tidal winds in the upper atmosphere over Jakarta, *J. Geophys. Res.*, *108*(A5), 1192, doi:10.1029/2002JA009528.

Vial, F., J. M. Forbes, and S. Miyahara (1991), Some transient aspects of tidal propagation, *J. Geophys. Res.*, *96*(A2), 1215–1224.

Vineeth, C., T. K. Pant, K. K. Kumar, and S. G. Sumod (2010), Tropical connection to the polar stratospheric sudden warming through quasi 16-day planetary wave, *Ann. Geophys.*, *28*(11), 2007–2013, doi:10.5194/angeo-28-2007-2010.

Wan, W., J. Xiong, Z. Ren, L. Liu, M. L. Zhang, F. Ding, B. Ning, B. Zhao, and X. Yue (2010), Correlation between the ionospheric WN4 signature and the upper atmospheric DE3 tide, *J. Geophys. Res.*, *115*, A11303, doi:10.1029/2010JA015527.

Waters, J. W., et al. (2006), The Earth Observing System Microwave Limb Sounder (EOS MLS) on the Aura satellite, *IEEE Trans*, *Geosci. Rem. Sen.*, *44*, 1075–1092.

Xiong, J., W. Wan, B. Ning, and L. Liu (2004), First results of the tidal structure in the MLT revealed by Wuhan Meteor Radar (30° 40′N, 114° 30′E), *J. Atmos. Sol. Terr. Phys.*, *66*(6–9), 675–682.

Yu, Y., W. Wan, B. Ning, L. Liu, Z. Wang, L. Hu, and Z. Ren (2012), Tidal wind mapping from observations of a meteor radar chain in December, 2011, *J. Geophys. Res.*, doi:10.1029/2012JA017976, in press.

Yuan, T., H. Schmidt, C. Y. She, D. A. Krueger, and S. Reising (2008), Seasonal variations of semidiurnal tidal perturbations in mesopause region temperature and zonal and meridional winds above Fort Collins, Colorado (40.6°N, 105.1°W), *J. Geophys. Res.*, *113* D20103, doi:10.1029/2007JD009687.

Yuan, T., B. Thurairajah, C. Y. She, A. Chandran, R. Collins, and D. Krueger (2012), Wind and temperature response of midlatitude mesopause region to the 2009 sudden stratospheric warming, *J. Geophys. Res.*, *117*, D09114, doi:10.1029/2011JD017142.

Yue, X. A., W. S. Schreiner, J. H. Lei, C. Rocken, D. C. Hunt, Y. H. Kuo, and W. X. Wan (2010), Global ionospheric response observed by COSMIC satellites during the January 2009 stratospheric sudden warming event, *J. Geophys. Res.*, *115*, A00G09, doi:10.1029/2010JA015466.